Tropical circulation and precipitation response to ozone depletion and recovery

2017 Environ. Res. Lett. 12 064011

(http://iopscience.iop.org/1748-9326/12/6/064011)

Environmental Research Letters

LETTER

Tropical circulation and precipitation response to ozone depletion and recovery

Stefan Brönnimann[1,2,9], Martín Jacques-Coper[1,2,3], Eugene Rozanov[4,5], Andreas M Fischer[3], Olaf Morgenstern[6], Guang Zeng[6], Hideharu Akiyoshi[7] and Yousuke Yamashita[7,8]

[1] Oeschger Centre for Climate Change Research, University of Bern, Falkenplatz 16, CH-3012 Bern, Switzerland
[2] Institute of Geography, University of Bern, Bern, Hallerstr. 12, CH-3012 Bern, Switzerland
[3] Federal Office of Meteorology and Climatology MeteoSwiss, Operation Center 1, P.O. Box 257, CH-8058 Zurich-Airport Switzerland
[4] Physical-Meteorological Observatory/World Radiation Center PMOD/WRC, Dorfstrasse 33, CH-7260 Davos Dorf, Switzerland
[5] Institute of Atmospheric and Climate Science, ETH Zurich, Universitätstr. 16, CH-8006 Zurich, Switzerland
[6] National Institute of Water and Atmospheric Research (NIWA), 301 Evans Bay Parade, Hataitai, Wellington 6021, New Zealand
[7] National Institute of Environmental Studies (NIES), 16-2 Onogawa, Tsukuba, Ibaraki Prefecture 305-0053, Japan
[8] Japan Agency for Marine-Earth Science and Technology (JAMSTEC), Yokohama, Japan
[9] Author to whom any correspondence should be addressed.

E-mail: stefan.broennimann@giub.unibe.ch

Keywords: South Pacific convergence zone, ozone depletion, southern annular mode, chemistry-climate modeling

Supplementary material for this article is available online

OPEN ACCESS

RECEIVED
21 December 2016

REVISED
11 May 2017

ACCEPTED FOR PUBLICATION
19 May 2017

PUBLISHED
13 June 2017

Abstract

Among the few well established changes in atmospheric circulation in recent decades are those caused by stratospheric ozone depletion. They include a strengthening and poleward contraction of the westerly atmospheric circulation over the Southern extratropics, i.e. a strengthening Southern Annular Mode (SAM), in austral spring and summer. Associated effects on extratropical temperature and precipitation and more recently subtropical precipitation have been documented and are understood in a zonal mean framework. We present zonally asymmetric effects of ozone depletion that reach into the tropics and affect atmospheric circulation and precipitation, including the South Pacific Convergence Zone (SPCZ), the most important rainband of the Southern Hemisphere. Using observation-based analyses and model simulations we show that over the 1961–1996 period, ozone depletion led to increased precipitation at the northern flank of the SPCZ and to decreased precipitation to the south. The effects originate from a flow pattern over the southwestern Pacific that extends equatorward and alters the propagation of synoptic waves and thus the position of the SPCZ. Model simulations suggest that anticipated stratospheric ozone recovery over the next decades will reverse these effects.

1. Introduction

The Intertropical Convergence Zone (ITCZ) consists of a zonally oriented part as well as of three diagonally oriented branches: the Southern Hemisphere Convergence Zones. Of these, the South Pacific Convergence Zone (SPCZ) is the most pronounced (Vincent 1994). It is an important component of the global hydrological cycle and the ocean freshwater budget (contributing to a pronounced sea-surface salinity front, see Linsley *et al* 2006) and is responsible for a substantial fraction of Southern Hemisphere precipitation variability (Cai *et al* 2012). The SPCZ is characterized by low-level convergence to the west of the South Pacific High. It is formed by transient synoptic waves originating south of that propagate eastward along the extratropical jet and are refracted equatorward. Upon reaching the SPCZ region, wave activity converges due to the decrease in zonal wind speed (Widlansky *et al* 2011, Matthews 2012, van der Wiel *et al* 2015). While intraseasonal variability of the SPCZ is related to the Madden–Julian Oscillation, its interannual-to-decadal variability depends on El Niño/Southern Oscillation (ENSO) and the Pacific Decadal Oscillation (Kidwell *et al* 2016). Large decadal variations in the SPCZ position since 1600 have been suggested based on ocean salinity proxies (Linsley *et al* 2006). The SPCZ is expected to change due to

Table 1. Overview of model simulations used (MME = Multi-Model Ensemble, CCE = CCMVal-2/CCMI Ensemble.

Project	Model (Reference)	Resolution	Ocean	ALL	noODS	MME	CCE
CASTRO	SOCOL (Schraner *et al* 2008)	T30L39	prescribed	9 × ALL	3 × noODS	29 simulations	17 simulations
CCMVal-2	CMAM (Scinocca *et al* 2008)	T31L71	coupled	3 × REF-B2	3 × SEN-B2b		
CCMVal-2	SOCOL (Schraner *et al* 2008)	T30L39	prescribed	1 × REF-B2	1 × SEN-B2b		
CCMI	CCSRNIES-MIROC3.2 (Akiyoshi *et al* 2016)	T42L34	prescribed	1 × REF-C2	1 × SEN-C2 fODS		
CCMI	NIWA-UKCA (Morgenstern *et al* 2013, 2014)	2.5° × 3.75°, L60	coupled	5 × REF-C2	2 × SEN-C2 fODS		

greenhouse warming (Cai *et al* 2012, Widlansky *et al* 2013). Effects of other forcing factors such as stratospheric ozone depletion have received little attention. Filling this gap is the aim of this paper.

Stratospheric ozone depletion is known to affect atmospheric circulation and precipitation in the extratropics. Thompson and Solomon (2002) and Gillett and Thompson (2003) showed that ozone depletion over Antarctica in spring induces a strengthening and poleward contraction of the westerly wind over the Southern extratropics, which can be understood as a strengthening of the Southern Annular Mode (SAM). These changes lead to an increase in precipitation at subpolar latitudes, a decrease at southern midlatitudes and an increase over (Thompson *et al* 2011). Warming in South Africa was found as a consequence of ozone depletion (Manatsa *et al* 2013). Kang *et al* (2011) found an increase in precipitation across the subtropics. In particular, Gonzalez *et al* (2014), exploring six climate models, attributed the 1960–1999 wetting trend over Southeastern South America to zonally asymmetric responses to stratospheric ozone depletion. A recent study (Manatsa *et al* 2016) hinted at an effect on East African precipitation, but little is still known about ozone depletion effects in the tropics.

Most previous studies on ozone depletion effects on atmospheric circulation and climate adopted a zonal mean perspective. In this paper we will take a zonally non-symmetric perspective to address the effect of ozone depletion on the SPCZ. For this purpose we use a set of chemistry-climate model simulations from a range of models, which allow us to directly address the effect in targeted simulations. In addition, we analyse several observation-based data sets to compare empirical evidence with our model simulation results.

2. Data and methods

2.1. Model simulations

Our main data set to study the effect of ozone depletion are simulations by the chemistry-climate model SOCOL (Schraner *et al* 2008). SOCOL is a combination of the Middle Atmosphere version of the European Centre/HAMburg Model 4 (MA-ECHAM4) spectral AGCM and the chemistry-transport model MEZON. It is run with T30 horizontal truncation and 39 vertical levels on a hybrid sigma-pressure coordinate system. The model spans the atmosphere from the surface to 0.01 hPa. An ensemble of nine simulations was performed in an 'all forcings' set-up (Fischer *et al* 2008, termed ALL) for the entire 20th century. The arguably most important boundary condition is sea-surface temperatures (SSTs) and sea ice, which are taken from HadISST1.1 (Rayner *et al* 2003). Ozone depleting substances were specified according to the CCMVal protocol (see Schraner *et al* 2008 for more detail). Furthermore, an additional ensemble of three simulations, branched off the ALL simulations, was performed with ozone depleting substances held fixed at their 1951 levels (termed noODS, see table 1).

In addition to these simulations, we used all available model simulations from the Chemistry-Climate Model Validation Activity for SPARC (CCMVal-2, Morgenstern *et al* 2010) and the Chemistry-Climate Model Initiative (CCMI, www.met.reading.ac.uk/ccmi/, Morgenstern *et al* 2017) that provide precipitation fields. In total, 17 simulations from four models were available (see table 1), covering the period 1960 to 2050. Note that the SOCOL simulations described above (Fischer *et al* 2008) were neither part of CCMVal-2 nor of CCMI, but SOCOL participated in CCMVal-2 with two additional simulations with a slightly different set-up (Morgenstern *et al* 2010). Note also that some models are coupled while others use prescribed SSTs and sea ice. Uncoupled simulations have the caveat that the possible role of SSTs in the climate system response is not captured, while they have the advantage of being more directly comparable with reanalyses and observations. We use the REF-B2 (in CCMVal-2, corresponding to IPCC's A1B scenarios in terms of greenhouse gases and WMO's A1 scenario for halogens, see SPARC 2010) or REF-C2 (in CCMI, corresponding to IPCC's RCP6.0 scenario and WMO's A1 scenario for halogens, see www.pa.op.dlr.de/CCMI/) scenario simulations as equivalent of ALL and the SEN-B2b or SEN-C2fODS, respectively, for the noODS scenario.

In addition to analyses of individual models, we also calculated a multi-model mean. It is based on the ALL minus noODS difference of each model, weighed with $(n^{-0.5} + m^{-0.5})^{-1}$, where n and m are the number

of members of ALL and noODS, to account for the dependence of the standard error on the ensemble size. We defined an ensemble comprising all CCMVal-2 and CCMI simulations as well as a multi-model ensemble that also includes the 9+3 SOCOL simulations. For precipitation, the ensemble means are expressed relative to a similarly weighted climatology (1961–90), i.e. as percentage anomalies.

2.2. Observation-based data sets

The South and Central Pacific region is not well observed, particularly when it comes to precipitation. We therefore used several observation based data sets. In order to assess the time when ozone depletion started, i.e. around 1960, we used some sparse station as well as reanalysis data for precipitation and atmospheric circulation. Precipitation station data for the region 55° S to 5° S and 170° E to 230° E were taken from the Global Historical Climatology Network (GHCN-Monthly, Peterson and Vose 1997) and were required to have at least 40 years of data in the 1958–2015 period and at least 30 years of data in the 1961–1996 period, which will later be used for most of the analyses. However, the data quality is largely unknown. For the period after 1979, we also used Global Precipitation Climatology Project (GPCP) combined satellite-based precipitation data Version 2.3 (Adler *et al* 2003).

For the atmospheric analyses we used the reanalyses JRA-55 (Kobayashi *et al* 2015) as well as NCEP/NCAR (Kalnay *et al* 1996) and 20CRv2c (Compo *et al* 2011). Results were similar, but because of large uncertainties in the tropical circulation in the latter two data sets (e.g. Pomposi *et al* 2015, Compo *et al* 2011), the main focus is on JRA-55.

2.3. Diagnostics and analysis procedure

The variables analysed in this paper are precipitation, 450 hPa geopotential height (a level common to both SOCOL and JRA-55; the variable is termed Z450 in the following), as well as 950 hPa wind. To address wave propagation across the South Pacific, we analysed *du/dx* (zonal stretching deformation, Widlansky *et al* 2011) at 200 hPa. Negative values indicate where the group velocity of propagating waves decreases and thus wave activity converges, representing a 'graveyard' of propagating disturbances (van der Wiel *et al* 2015).

The analysis sequence was as follows. After analysing trends in model simulations and observation-based data, we addressed the ozone-induced change in the simulations as the linear trend in the difference ALL-noODS. The ozone-induced change in the observation-based data was extracted using a multiple regression model (see below). After finding a consistent response in the SPCZ region, we supplemented this 'forward' approach with a 'backward' analysis. We defined a precipitation index for the identified SPCZ signature and regressed the global fields onto that index (both in simulations and observation-based data) to confirm the high-latitude origin and to elucidate the possible mechanism. This led to the identification of a likely dynamical origin of the response in southern midlatitude geopotential height. We finally defined an index for that feature and again regressed the global fields onto this index (in simulations and observation-based data), confirming its relation foreward to the SPCZ and backward to high-latitude geopotential height changes.

We focus our analysis on October to December, which is the period immediately following the ozone loss season and the start of the summer rainfall season in the SPCZ. Analyses for December–February or October–February (shown in the supplement) gave similar results.

Linear trends were calculated using a least-squares regression. Significance was tested using the Mann-Kendall test with $p < 0.05$. Following Thompson and Solomon (2002) all trends in this paper are multiplied by the period length (i.e. they are expressed as changes over the period of trend calculation).

2.4. Total column ozone gradient

As a measure for the ozone forcing, which is understood to result from an intensified latitudinal heating gradient in the lower stratosphere, we used the difference in total column ozone between the high- and mid-latitudes with a one-month lead time (i.e. September–November). As no total column ozone observations are available poleward of 80° S in September, we chose the regions 60° S–80° S and 30° S–50° S. The difference between the two zonal bands is termed dTOZ. Prior to 1979, the data were taken from the HISTOZ data set (Brönnimann *et al* 2013), which is a nine member ensemble assimilation of historical ground-based and satellite (BUV) data into the ALL simulations. For each year we chose the assimilated member that was closest to all observations south of 30° S in terms of Eucledian distance. From 1979 onward we used total column ozone data from JRA-55, which agrees very well with SBUV data but is spatio-temporally complete.

The time series of dTOZ from observation-based data, ALL and noODS (figure 1), reveal that ozone depletion began already around 1960 (see also Schneider *et al* 2015). dTOZ declined until the mid 1990s, stronger in ALL than in observation-based data. While the observed dTOZ remains at a low level for another 10 years, the simulated recovery starts after around 1994. Based on this, we chose the 35 year period of 1961−96 as our analysis period, which captures the entire ozone depletion period and avoids the very large 1997/98 El Niño event (analyses over different time periods gave very similar results). In addition, we also performed analyses over the 1979−96 period, which enables using the satellite-based precipitation data and facilitates the comparison with other studies.

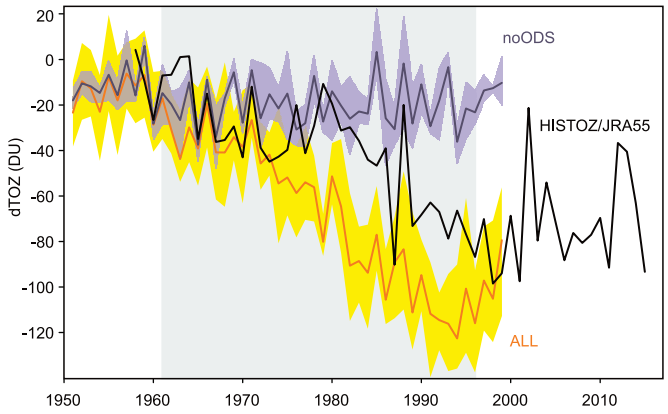

Figure 1. October-to-December averages of dTOZ in observations-based data (HISTOZ) as well as in the ALL and noODS simulations (thick line gives the ensemble mean, the shading indicates the range). The grey background colour denotes the period of analysis in this study.

2.5. Regression

We applied a multiple linear regression to October–December averaged fields in observation-based data sets over the 1958–2015 period (1979–2015 for GPCP data). We used eight predictor variables that were based on monthly data averaged over September–November. In addition to dTOZ, we used CO_2 concentrations at Mauna Loa (NOAA) as well as six SST indices (HadISST1.1), which should remove effects of oceanic variability. We used two indices per ocean basin, namely NINO3.4 (averaged SSTs over the area [170° W−120° W, 5° S−5° N]), the unfiltered Tripole Pacific Index (Henley *et al* 2015), the Indian Ocean Zonal Mode ([50° E–70° E, 10° S−10° N] minus [90° E–110° E, 10° S−10° N]), the Indian Ocean Basin Mode [40° E–110° E, 20° S−20° N], the Atlantic Nino index [20° W−0° W, 3° S−3° N], and the Atlantic Meridional Mode (obtained from NOAA ESRL/PSD). To estimate the ozone-induced contribution, we then multiplied the coefficients for dTOZ with its trend over the 1961−96 period to derive a change for the 1961−96 period.

It is important to check possible multicollinearity of dTOZ. The correlation between dTOZ and CO_2 concentrations is −0.729, while it is close zero with all other variables. The Variance Inflation Factor is 2.33, which indicates that multicollinearity should not have a large effect. We tested various model set-ups, using different combinations of variables or detrending all variables while omitting greenhouse gases. Results (figure S1 available at stacks.iop.org/ERL/12/064011/mmedia for Z450) are almost identical for all regression models.

3. Results and discussion

3.1. Model evaluation and precipitation trends

For addressing ozone depletion effects on tropical precipitation, it is important that the model realistically simulates the precipitation climatology as well as the known effects on the high-latitude atmospheric circulation. In fact, 1961−90 precipitation climatologies for the October–December season (figure 2) from JRA-55 and ALL agree very well with each other. The same is true for climatologies of 200 hPa *du/dx*. Thus, the model simulates the SPCZ and the main processes responsible for its climatology well.

A previous study (Brönnimann *et al* 2015) also found that the ALL simulations realistically reproduce shifts in the ITCZ in the second half of the 20th century. Furthermore, we reproduced the results by Thompson and Solomon (2002), who analysed the change in atmospheric circulation and temperature over the Southern extratropics over the 1969−99 period for December–February. The change in ALL fits well with the observations shown in that paper (figure S2, from Brönnimann 2015), although magnitudes are smaller. The trend (expressed as change over the considered time period) completely disappears in the noODS simulations. The model thus produces a consistent response of the SAM to stratospheric ozone depletion.

Over the 1961−96 period, October–December precipitation in JRA-55 increased by up to 50% (of its 1961−90 average) in the northeastern flank of the SPCZ (figure 2). This number is confirmed with station data from Hérététué, Atuona and Rikitea (French Polynesia; dots in figure 2). Precipitation decreased in the southwestern part and further to the south (global maps in figure S3). The general pattern of the trend around the SPCZ as well as the trend at subpolar latitudes is well reproduced in the ALL simulations. Although there are differences in the subtropical eastern Pacific and around New Zealand and in the southeastern Pacific, the model simulations appear suitable for analysing precipitation trends in the SPCZ region.

3.2. Ozone depletion-induced trends

The trend in the atmospheric circulation differences between ALL and noODS over the 1961–96 period

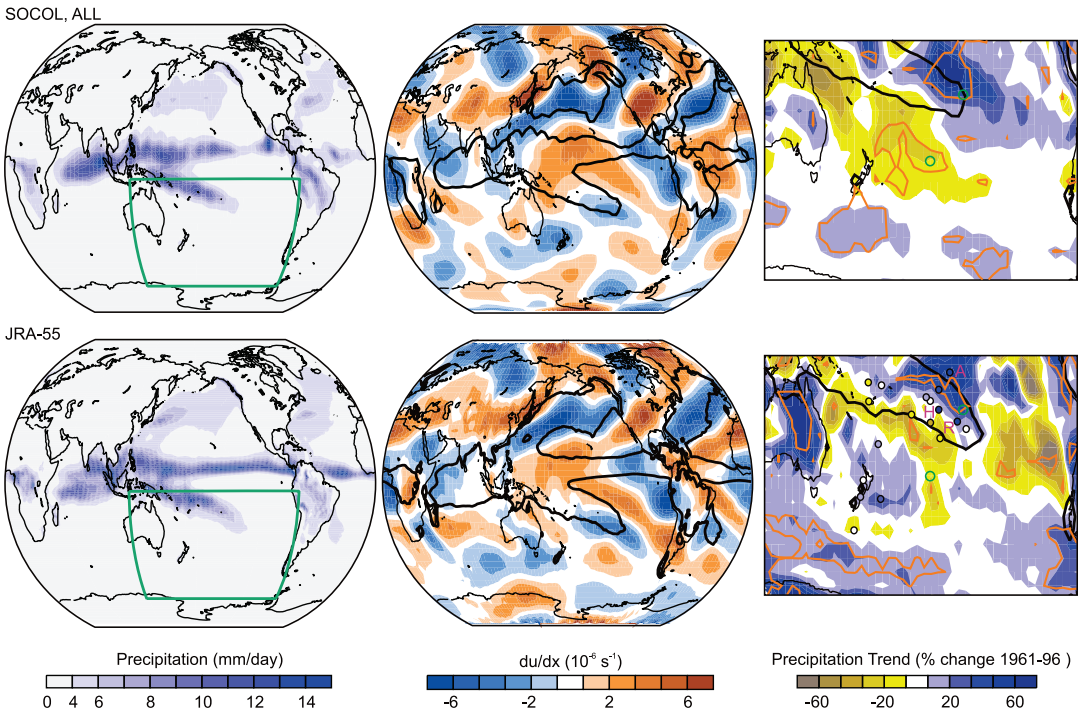

Figure 2. October-to-December averaged precipitation (left) and *du/dx* at 200 hPa (middle) in SOCOL ALL (top) and JRA-55 (bottom). Right: Linear trend in October–December averaged precipitation over the period 1961−96, expressed as percentage change from the 1961−90 average over the trend period. Thick black lines indicate average precipitation of 4 mm day^{-1} for orientation. Orange lines indicate a *p*-value of 0.05. Dots in the upper right panel denote observations (H, A, and R stand for Héréhérétué, Atuona and Rikitea, respectively). Green dots indicate the points whose difference defines ΔR_{SPCZ}.

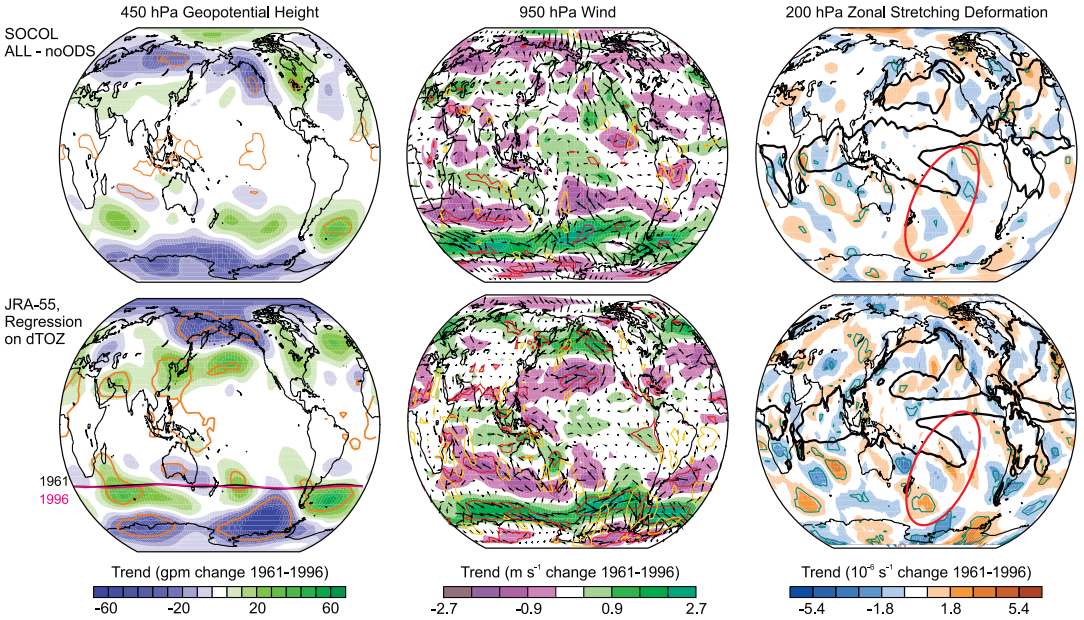

Figure 3. Ozone depletion-induced change in October–December, 1961−96, in climate model simulations and a regression approach. Results are shown for 450 hPa GPH, 950 hPa wind (colours indicate zonal wind), and 200 hPa zonal stretching deformation *du/dx*. The top row shows linear trends in the ensemble mean difference of ALL-noODS in SOCOL simulations, the bottom row shows the change due to dTOZ in a regression approach using JRA-55. Both trends are expressed as change over the 1961−96 period. Thin lines (red and yellow for zonal and meridional wind, respectively) indicate a *p*-value of 0.05, black and pink lines in the bottom left panel indicate the position of the 6400 gpm isoline from the regression.

illustrates the effect of ozone depletion. The patterns for Z450 and 950 hPa wind (figure 3, top) show a strengthening of the westerlies near 60° S and decreasing (increasing) Z450 poleward (equatorward). In *du/dx*, a northwest-to-southeast tilted pattern appears over the South Pacific (red ellipses in figure 3), with significantly negative values at the SPCZ elongation.

The circulation response to ozone depletion in JRA-55, as obtained by the regression approach

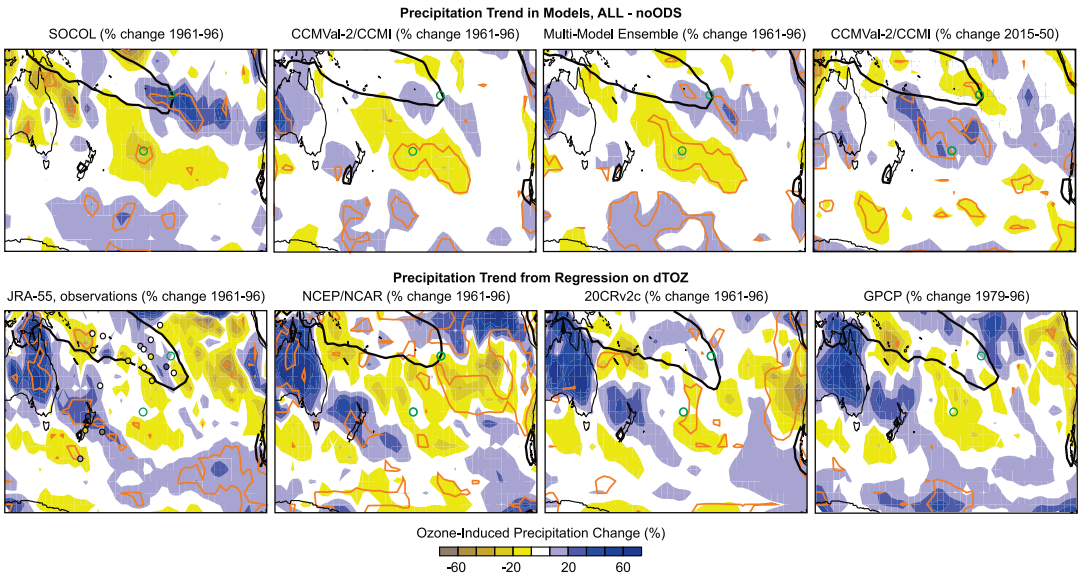

Figure 4. Ozone depletion-induced change in October–December, 1961−96, in (top) climate model simulations (trend in ALL minus noODS) and (bottom) in a regression approach. Results are shown for different model ensembles and different observation-based data sets (station observations are shown in the bottom left panel). Also shown is the simulated change due to future ozone recovery (2015−50) in the CCMVal-2/CCMI ensemble and the regression result for GPCP satellite-based precipitation (1979–96). All trends are expressed as % changes over the trend period. The black line shows the 4 mm day^{-1} isoline from the corresponding climatology. Orange lines indicate *p*-values of 0.05. Dots in the middle left panel indicate observations. Green dots indicate the points whose difference defines ΔR_{SPCZ}.

(figure 3, bottom), shows close similarities with the SOCOL results. Changes in GPH are similar over the southern mid- and high-latitudes, i.e. a decrease over Antarctica and an increase in three areas southeast of the continents. Good agreement is also found for 950 hPa wind. All main features are highly significant. A very similar pattern as in the model results is also found for *du/dx*, although the position slightly differs. Model and the observation-based approaches thus both suggest that ozone depletion altered the atmospheric flow over the southern mid- and high-latitudes and into the tropical Pacific region.

The corresponding trend patterns in precipitation (figure 4) are more variable. In the SOCOL simulations, zonal signatures appear at southern mid and high latitudes (global maps in figure S4). Over the Pacific, we find an elongation of the SPCZ into the South Pacific and a decrease in precipitation to the south; both features are statistically significant ($p<0.05$). An analysis of the individual ALL members (expressed relative to the noODS ensemble mean) shows that this response is robust. This is confirmed by studying the individual CCMVAl-2/CCMI models (figure S4), although the SPCZ itself differs between models. The CCMVal-2/CCMI ensemble (figure 4) again shows an elongation of the SPCZ and a significant drying to the south. Finally, the multi-model ensemble (encompassing SOCOL and the CCMVal-2/CCMI ensemble) clearly shows that the SPCZ is altered.

The ozone-induced precipitation change in observation-based data (figures 4, S5) agrees with the model results despite variability. The regression results indicate a wetting at subpolar latitudes, a drying south of the SPCZ, and a precipitation increase in or just north of the tip of the SPCZ, although the latter is not significant. The precipitation station observations only partly show the signature found in JRA-55, but they also do not contradict the result. The NCEP/NCAR and 20CRv2c show similar results as JRA-55 (figure S5). The same analysis (but only post-1979) was also performed with GPCP data (figure 4) and confirmed the main patterns, although the significance level is not reached for that short period.

Taking the circulation and the precipitation response together, both in the models and in observation-based analysis, we find that the response of the Pacific is not zonally oriented, but shows a clear northwest-to-southeast tilt. In the models, the pattern is slightly shifted (larger response near the tip of the SPCZ) relative to the regression approach (larger response in the northern flank of the tip).

3.3. Relevance for past and future precipitation trends

According to our results, ozone depletion induced precipitation changes in the SPCZ region on the order of −25 to 40% over the 1961–96 period. How important is this for precipitation trends? In JRA-55, SOCOL and CCMVal-2/CCMI, the total (figures 2, S6) and ozone-induced precipitation changes (figure 4) have similar patterns. In the SPCZ region, ozone depletion explains about half of the total trend. The precipitation increase in the northeastern part and the tip of the SPCZ and the decrease in the southwestern part 1961−96 can therefore, to a considerable extent, be explained by ozone depletion.

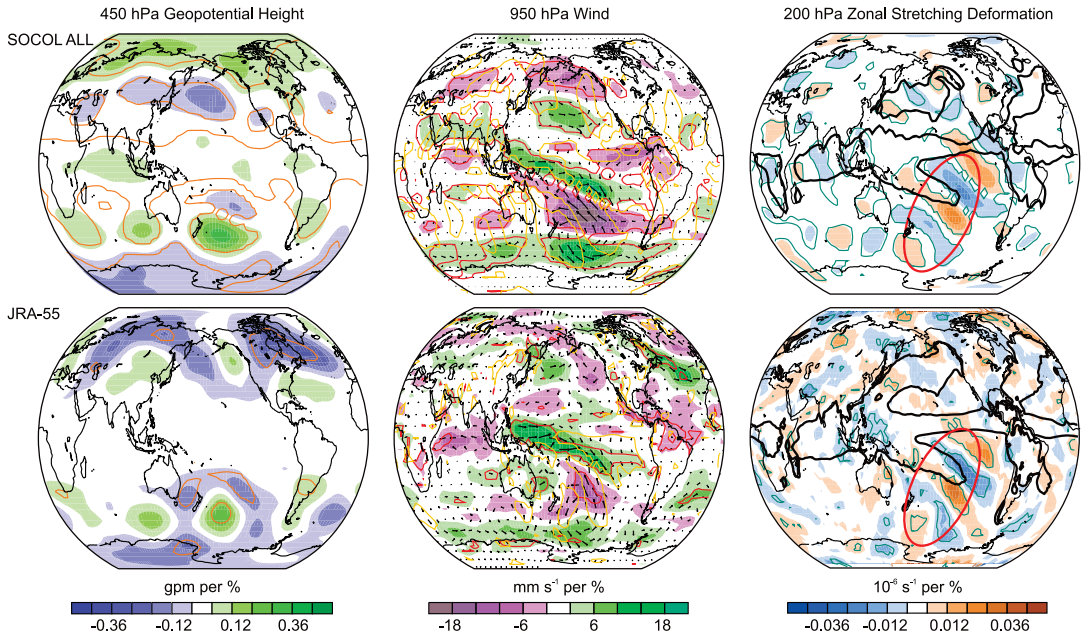

Figure 5. Regression of October–December averaged SOCOL ALL (top) and JRA-55 (bottom) fields onto ΔR_{SPCZ}. Results are shown for 450 hPa GPH, 950 hPa wind (colours indicate zonal wind), and 200 hPa zonal stretching deformation *du/dx*. Thin lines (red and yellow for zonal and meridional wind, respecitvely) indicate a *p*-value of 0.05, the red ellipses are for orientation. Thick black lines indicate precipitation of 4 mm day^{-1}.

During the past 20 years with stable but low ozone levels (1996–2015), precipitation trends in the SPCZ region were different than in the earlier period (although this period is very short; figure S3). With ozone recovery now underway, we expect the effects of ozone depletion to reverse. In particular, we expect a decreased precipitation in the northern tip of the SPCZ and increased precipitation to the south, which might have societal impacts in the island countries affected by the SPCZ variability (e.g. Cai *et al* 2012). Over the 2015−50 period in the CCMVal-2/CCMI ensemble (figures 4, S6), the ozone-induced change is almost a mirror image of that over the 1961−96 period, confirming the robustness of our results. The changes in the SPCZ are statistically significant.

3.4. Mechanism of the teleconnection

In order to analyse the mechanism of this response, we defined an index ΔR_{SPCZ} as the difference in precipitation between the northeastern part of the SPCZ and the area south of the SPCZ (19° S, 135° W minus 37.5° S, 150° W). This index best expresses the common signature in all analyses (e.g. it is positive for each of the 9 members in SOCOL, statistically significant for 3 members). We then regressed atmospheric fields onto ΔR_{SPCZ} both in ALL and in JRA-55, i.e. we analysed in a 'backward' manner, which flow features are likely to cause changes in the tip of the SPCZ (figure 5).

The patterns are similar in ALL and in JRA-55. They are also similar to those attributed to ozone depletion, but the positive node in Z450 over the South Pacific as well as the wave pattern in *du/dx* over the South Pacific are more pronounced in this case. Thus the forward analysis (studying the consequences of ozone depletion) and the backward analyses (exploring the causes for changes in the SPCZ) yield very similar results, both in models and in observation-based analyses.

The figure implies that the pattern originates in the southern South Pacifc region, from where a wave pattern emerges. Specifically, a trough-ridge pattern near New Zealand appears in the 6400 gpm isoline of Z450 (figure 3). We therefore defined a longitudinal index of Z450 along 40° S (ΔZ_{SP} = Z450 [40° S, 110° E + 40° S, 190° E − 40° S, 150° E + 40° S, 230° E] in September–November) and regressed atmospheric fields onto that index. Results (figure 6) reproduce the flow pattern over Antarctica as well as in the SPCZ region, both in JRA-55 and in ALL (but again with a slight shift in the SPCZ region between the two). Those ALL members (relative to noODS) that produce a strong trend in ΔZ_{SP} also produce strongest changes in ΔR_{SPCZ}.

For comparison, we also regressed October–December averaged fields from JRA-55 onto a September–November averaged SAM index of Marshall (2003), (figure S7). Results show pronounced, zonally symmetric changes in wind and Z450 (though with a clear node southeast of New Zealand). We also find an imprint in *du/dx* and a slight precipitation increase in a narrow zone in the tip of the SPCZ. However, compared to the pattern for ΔZ_{SP} (figure 6), the SAM imprint is much more zonally symmetric and confined to high- and mid-latitudes.

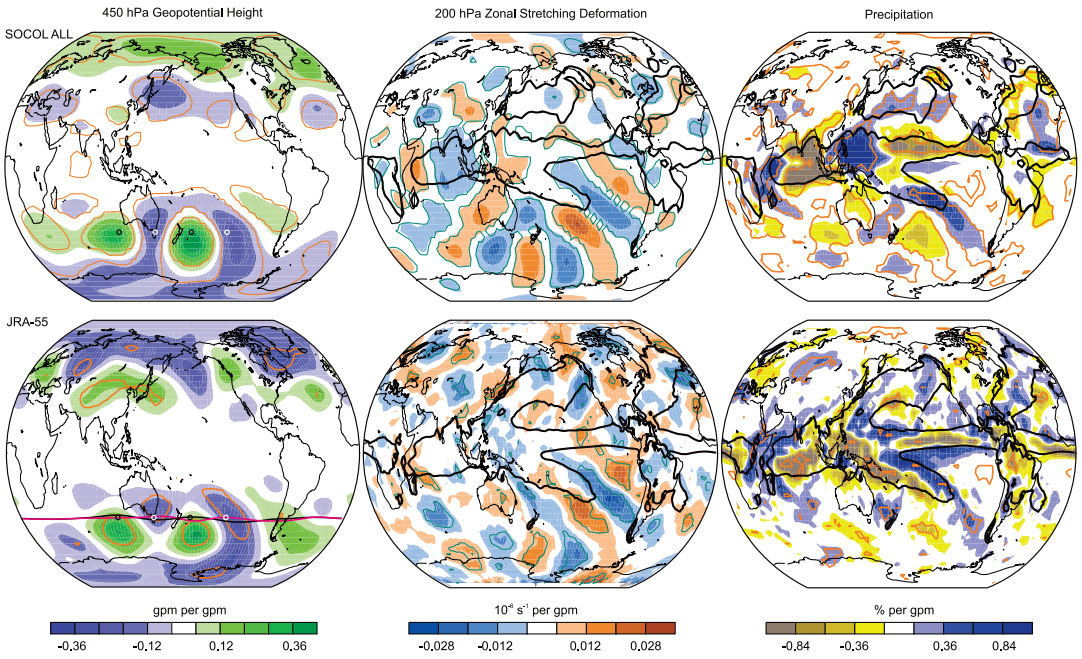

Figure 6. Regression of October–December averaged SOCOL ALL (top) and JRA-55 (bottom) fields onto ΔZ_{SP}. Results are shown for 450 hPa GPH, 950 hPa wind (colours indicate zonal wind), and 200 hPa zonal stretching deformation *du/dx*. Thin lines (red and yellow for zonal and meridional wind, respecitvely) indicate a *p*-value of 0.05, the red ellipses are for orientation. Thick black lines indicate precipitation of 4 mm day^{-1}. Black and pink lines in the bottom left panel indicate the position of the 6400 gpm isoline from the regression.

4. Discussion

In the extratropics and subtropics, our results agree well with previous studies (e.g. Thompson and Solomon 2002, Gillett and Thompson 2003, Thompson *et al* 2011, Kang *et al* 2011, Purich and Son 2012, Manatsa *et al* 2013, Schneider *et al* 2015). This mechanism is understood in a zonal mean framework: A positive SAM induces a poleward momentum flux, which in turn induces a meridional circulation cell that causes the drying near 45° S and the wetting near 60° S (Kang *et al* 2011, Hendon *et al* 2014). Kang *et al* (2011) found an adjacent meridional cell that leads, in a zonal mean sense, to uplift and increased precipitation in the subtropics. This is confirmed in our study. However, our signature over the SPCZ region differs from the latter study, which analysed the 1979–2000 period in the CMAM model. This requires further analyses as CMAM simulations are also in our analysis (3 ALL, 2 noODS) and agree with the SOCOL results in that respect, even when analysed only for the 1979–2000 period (figure S4).

The signature in the SPCZ cannot be explained in a zonally averaged framework. The two main areas of interest are the Indian Ocean south of Australia and the western Pacific. The former is the origin of synoptic waves which then propagate along the jet across Australia and are refracted equatorward. The latter is the region where wave activity converges in the SPCZ region. The positive Z450 signatures east of the southern continents suggest that ozone depletion weakened, and even reversed, the troughs behind the Andes and New Zealand. Interaction of the weakened (southward shifted) westerlies at these latitudes with orography remains to be studied. The change in ΔZ_{SP} can be understood as a change towards a trough (ridge) west (east) of New Zealand (pink and black lines in figure 6 indicate the 6400 gpm isoline for $\Delta Z_{SP} = 100$ gpm and $\Delta Z_{SP} = -100$ gpm, respectively). This configuration might have changed the wave propagation across the South Pacific, as evidenced in *du/dx*. Synoptic-scale studies are necessary to further elaborate this link.

Are these changes part of the SAM? Our analysis shows the classical SAM features, which are described in the literature (Gillett *et al* 2006, Villalba *et al* 2012). The response in *du/dx* and precipitation is similar to the ozone-induced pattern, but much weaker and thus can only partly explain it. Recent work has also emphasized zonally asymmetric aspects of the SAM and its relation to tropical circulation (Ding *et al* 2012, Fogt *et al* 2012, Clem and Renwick 2015). Our results further demonstrate the importance of zonally asymmetric flow patterns over the southwestern Pacific. The same might hold for the South Atlantic and South Indian Ocean, which were not the focus of our study.

5. Conclusions

The effects of ozone depletion on atmospheric circulation include a zonally asymmetric pattern over the South Pacific that originates from a ridge east of New Zealand and propagates into the tropics. It alters the shape and position of the South Pacific Conver-

gence Zone (SPCZ). Using observation-based analyses and model simulations, we show that, over the 1961–96 period, ozone depletion led to increased precipitation at the northern flank of the SPCZ and decreased precipitation to the south. This trend is expected to reverse over the next decades. Our study demonstrates that ozone depletion was an important driver of climatic changes in the tropical South Pacific in the past, and so will ozone recovery be in the future. The study also presents a new teleconnection mechanism between the stratospheric polar vortex over Antarctica and tropical circulation. While the presented case is an 'anthropogenic teleconnection', the mechanism might also be relevant for other forcing mechanisms known to affect the polar vortex such as solar or volcanic forcing.

Acknowledgments

We acknowledge the joint WCRP SPARC/IGAC Chemistry-Climate Model Initiative (CCMI) for organizing and coordinating the model data analysis activity, and the British Atmospheric Data Centre (BADC) for collecting and archiving the CCMI and CCMVal model output. The work was funded by the Swiss National Science Foundation (project FUPSOL2) and EU FP7 project ERACLIM-2. HA acknowledges the Environment Research and Technology Development Fund, Ministry of Environment, Japan (2–1303) and NEC–SX9/A(ECO) computers at CGER, NIES. This research was supported by the New Zealand Government's Strategic Science Investment Fund (SSIF) through the NIWA programme CACV. OM acknowledges funding from the Royal Society of New Zealand Marsden Council (12-NIW-006). The authors wish to acknowledge the contribution of NeSI high-performance computing facilities to the results of this research. NZ's national facilities are provided by the NZ eScience Infrastructure and funded jointly by NeSI's collaborator institutions and through the Ministry of Business, Innovation & Employment's Research Infrastructure programme. URL www.nesi.org.nz. The authors acknowledge the UK MetOffice for use of the MetUM. We thank all data providers and Dave Thompson, Olivia Romppainen, and Matthias Röthlisberger for discussions. Support for the Twentieth Century Reanalysis Project dataset is provided by the US Department of Energy, Office of Science Innovative and Novel Computational Impact on Theory and Experiment (DOE INCITE) program, and Office of Biological and Environmental Research (BER), and by the National Oceanic and Atmospheric Administration Climate Program Office.

References

Adler R F *et al* 2003 The version 2 Global Precipitation Climatology Project (GPCP) monthly precipitation analysis (1979-present) *J. Hydrometeorol.* **4** 1147–67

Akiyoshi H, Nakamura T, Miyasaka T, Shiotani M and Suzuki M 2016 A nudged chemistry-climate model simulation of chemical constituent distribution at northern high-latitude stratosphere observed by SMILES and MLS during the 2009/2010 stratospheric sudden warming *J. Geophys. Res.* **121** 1361–80

Brönnimann S, Bhend J, Franke J, Flückiger S, Fischer A M, Bleisch R, Bodeker G, Hassler B, Rozanov E and Schraner M 2013 A global historical ozone data set and prominent features of stratospheric variability prior to 1979 *Atmos. Chem. Phys.* **13** 9623–39

Brönnimann S 2015 Climatic changes since 1700 *Advances in Global Change Research* vol 55 (Cham: Springer) (https://doi.org/10.1007/978-3-319-19042-6)

Brönnimann S, Fischer A M, Rozanov E, Poli P, Compo G P and Sardeshmukh P D 2015 Southward shift of the northern tropical belt from 1945 to 1980 *Nat. Geosci.* **8** 969–74

Cai W *et al* 2012 More extreme swings of the South Pacific convergence zone due to greenhouse warming *Nature* **488** 365–69

Clem K and Renwick J 2015 Austral spring Southern Hemisphere circulation and temperature changes and links to the SPCZ *J. Clim.* **28** 7371–84

Compo G P *et al* 2011 The Twentieth Century Reanalysis Project *Q. J. R. Meteorol. Soc.* **137** 1–28

Ding Q, Steig E J, Battisti D S and Wallace J M 2012 Influence of the tropics on the Southern Annular Mode *J. Clim.* **25** 6330–48

Fischer A M *et al* 2008 Interannual-to-decadal variability of the stratosphere during the 20th century: ensemble simulations with a chemistry-climate model *Atmos. Chem. Phys.* **8** 7755–77

Fogt R L, Jones J M and Renwick J 2012 Seasonal zonal asymmetries in the southern annular mode and their impact on regional temperature anomalies *J. Clim.* **25** 6253–70

Gillett N P and Thompson D W J 2003 Simulation of recent Southern Hemisphere climate change *Science* **302** 273–75

Gillett N P, Kell T D and Jones P D 2006 Regional climate impacts of the Southern Annular Mode *Geophys. Res. Lett.* **33** L23704

Gonzalez P L M, Polvani L M, Seager R and Correa G J P 2014 Stratospheric ozone depletion: a key driver of recent precipitation trends in south-eastern South America *Clim. Dyn.* **42** 1775–92

Hendon H H, Lim E-P and Nguyen H 2014 Seasonal variations of subtropical precipitation associated with the southern annular mode *J. Clim.* **27** 3446–60

Henley B J, Gergis J, Karoly D J, Power S, Kennedy J and Folland C K 2015 A tripole index for the Interdecadal Pacific Oscillation *Clim. Dyn.* **45** 3077–90

Kalnay E *et al* 1996 The NCEP/NCAR 40-year reanalysis project *Bull. Am. Meteorol. Soc.* **77** 437–70

Kang S M, Polvani L M, Fyfe J C and Sigmond M 2011 Impact of polar ozone depletion on subtropical precipitation *Science* **332** 951–54

Kidwell A, Lee T, Jo Y-H and Yan X-H 2016 Characterization of the variability of the South Pacific convergence zone using satellite and reanalysis wind products *J. Clim.* **29** 1717–32

Kobayashi S *et al* 2015 The JRA-55 reanalysis: general specifications and basic characteristics *J. Meteorol. Soc. Jpn.* **93** 5–48

Linsley B K, Kaplan A, Gouriou Y, Salinger J, deMenocal P B, Wellington G M and Howe S S 2006 Tracking the extent of the South Pacific convergence zone since the early 1600s *Geochem. Geophys. Geosyst.* **7** Q05003

Manatsa D, Morioka Y, Behera S K, Yamagata T and Matarira C H 2013 Link between Antarctic ozone depletion and summer warming over southern Africa *Nat. Geosci.* **6** 934–39

Manatsa D, Mudavanhu C, Mushore T D and Mavhura E 2016 Linking major shifts in East Africa 'short rains' to the Southern Annular Mode *Int. J. Climatol.* **36** 1590–99

Marshall G J 2003 Trends in the Southern Annular Mode from observations and reanalyses *J. Clim.* **16** 4134–43
Matthews A J 2012 A multiscale framework for the origin and variability of the South Pacific convergence zone *Q. J. R. Meteorol. Soc.* **138** 1165–78
Morgenstern O *et al* 2010 Review of the formulation of present-generation stratospheric chemistry-climate models and associated external forcings *J. Geophys. Res.* **115** D00M02
Morgenstern O *et al* 2013 Impacts of climate change ozone recovery and increasing methane on surface ozone and the tropospheric oxidizing capacity *J. Geophys. Res.* **118** 1028–41
Morgenstern O, Zeng G, Dean S M, Joshi M, Abraham N L and Osprey A 2014 Direct and ozone mediated forcing of the Southern Annular Mode by greenhouse gases *Geophys. Res. Lett.* **41** 9050–57
Morgenstern O *et al* 2017 Review of the global models used within the Chemistry-Climate Model Initiative (CCMI) *Geosci. Model Dev.* **10** 639–71
Peterson T C and Vose R S 1997 An overview of the Global Historical Climatology Network temperature database *Bull. Am. Meteorol. Soc.* **78** 2837–49
Pomposi C, Kushnir Y and Giannini A 2015 Moisture budget analysis of SST-driven decadal Sahel precipitation variability in the twentieth century *Clim. Dyn.* **44** 3303–21
Purich A and Son S-W 2012 Impact of antarctic ozone depletion and recovery on Southern Hemisphere precipitation evaporation and extreme changes *J. Clim.* **25** 3145–54
Rayner N A *et al* 2003 Global analyses of SST sea ice and night marine air temperature since the late nineteenth century *J. Geophys. Res.* **108** 4407
Schneider D, Deser C and Fan T 2015 Comparing the impacts of tropical SST variability and polar stratospheric ozone loss on the Southern Ocean westerly winds *J. Clim.* **28** 9350–72
Schraner M *et al* 2008 Technical note: chemistry-climate model SOCOL: Version 2.0 with improved transport and chemistry/microphysics schemes *Atmos. Chem. Phys.* **8** 5957–74
Scinocca J F, McFarlane N A, Lazare M, Li J and Plummer D 2008 Technical note: the CCCma third generation AGCM and its extension into the middle atmosphere *Atmos. Chem. Phys.* **8** 7055–74
SPARC 2010 *SPARC CCMVal Report on the Evaluation of Chemistry-Climate Models* ed V Eyring, T Shepherd and D Waugh SPARC Report No. 5, WCRP-30/2010, WMO/TD-No. 40
Thompson D W J and Solomon S 2002 Interpretation of recent Southern Hemisphere climate change *Science* **296** 895–99
Thompson D W J, Solomon S, Kushner P J, England M H, Grise K M and Karoly D J 2011 Signatures of the Antarctic ozone hole in Southern Hemisphere surface climate change *Nat. Geosci.* **4** 741–49
van der Wiel K, Matthews A J, Stevens D P and Joshi M M 2015 A dynamical framework for the origin of the diagonal South Pacific and South Atlantic convergence zones *Q. J. R. Meteorol. Soc.* **141** 1997–10
Villalba R *et al* 2012 Unusual Southern Hemisphere tree growth patterns induced by changes in the southern annular mode *Nat. Geosci.* **5** 793–98
Vincent D G 1994 The South Pacific Convergence Zone (SPCZ): a review *Mon. Weath. Rev.* **122** 1949–70
Widlansky M J, Timmermann A, Stein K, McGregor S, Schneider N, England M H, Lengaigne M and Cai W 2013 Changes in South Pacific rainfall bands in a warming climate *Nat. Clim. Change* **3** 417–23
Widlansky M J, Webster P J and Hoyos C D 2011 On the location and orientation of the South Pacific Convergence Zone *Clim. Dyn.* **36** 561–78